

Optical-Cavity Manipulation Strategies of Conical Intersections Mediated Singlet Fission Systems

Kewei Sun^{1,2}, Maxim F. Gelin^{1,2}, Kaijun Shen², and Yang Zhao^{2*}

¹*School of Science, Hangzhou Dianzi University, Hangzhou 310018, China*

²*School of Materials Science and Engineering, Nanyang Technological University, Singapore 639798, Singapore*

(Dated: March 14, 2024)

We offer a theoretical perspective on simulation and engineering of polaritonic conical-intersection-driven singlet-fission (SF) materials. Using rubrene as an example and applying the numerically accurate Davydov-Ansatz methodology, we derive dynamic and spectroscopic responses of the system and demonstrate key mechanisms capable of SF manipulation, viz. cavity-induced enhancement/weakening/suppression of SF, population localization on the singlet state via engineering of the cavity-mode excitation, polaron/polariton decoupling, collective enhancement of SF. We outline unsolved problems and challenges in the field, and share our views on the development of the future lines of research. We emphasize the significance of careful modeling of cascades of polaritonic conical intersections in high excitation manifolds and envisage that collective geometric phase effects may remarkably affect the SF dynamics and yield. We argue that microscopic interpretation of the main regulatory mechanisms of the polaritonic conical-intersection-driven SF can substantially deepen our understanding of this process, thereby providing novel ideas and solutions for improving conversion efficiency in photovoltaics.

With the constant emergence of novel ideas, concepts, and breakthroughs, the boundaries between disciplines have become increasingly blurred, leading to the ascent of highly interdisciplinary fields. One such example is the intersection of molecular physics/chemistry, photonics, and materials science, which gave a birth to optical cavity molecular science and optical cavity materials science [1–3]. By harnessing the strong coupling between photonic modes of an optical cavity (or localized surface plasmon modes of nanoscale structures) and electronic/vibrational degrees of freedom (DOFs) of molecular systems, hybrid electron-vibration-photonic states can be formed [4–7] and characterized by means of nonlinear ultrafast spectroscopy [8, 9].

Quantum electrodynamics (QED), the theoretical tool indispensable for modeling/understanding cavity-induced phenomena, was developed in the 1948-1949s [10–13] and recently heralded its 75th anniversary (see [14] for a mini review). The polariton line was observed in the ZnO crystal in 1965 [15]. The light-matter strong-coupling regime was demonstrated on phonons in the thin LiF film in 1975 [16] and realized for a single Rydberg atom in the superconducting cavity in 1985 [17, 18]. In the early 1990s, the strong coupling between excitons and photonic modes was experimentally demonstrated in semiconductor quantum dots [19]. Since then, formation of polaritons owing to the strong coupling between optical-cavity/surface-plasmon modes and molecular excitons in various systems and under different scenarios have attracted significant attention, and a novel area of research known as polaritonic photo-physics/photochemistry (PPP) has been established [1–

9].

PPP deals with a large variety of processes, for example photoisomerization [20, 21], photoinduced reactions in optical cavities or on metal substrates [22, 23], electron and energy transfer processes [24, 25]. Several intriguing phenomena have been discovered in the PPP studies. For instance, cavity-induced modification of the excitonic transport occurs mainly through the delocalized polariton modes rather than tunneling [26]. Cavities may enhance the exciton coherence length, as well as alter and even eliminate vibronic coupling in J-aggregates [27, 28]. Organic semiconductors showcase increasing conductivity in optical cavities [29], and Raman scattering is enhanced owing to the presence of polaritons [30]. Strong light-matter coupling has been experimentally demonstrated for chromosomes of photosynthetic bacteria [31], photosynthetic complexes [32], and even for living *Chlorobaculum tepidum* bacteria [33]. These and other phenomena demonstrate that PPP holds potential for exciting practical applications, e. g., for engineering novel quantum materials [34] and development of polaritonic devices [35].

One of such applications, which holds a great promise for artificial light harvesting [36, 37] and can be substantially improved by the PPP machinery, is singlet fission (SF). It is a spin-allowed photophysical process discovered over fifty years ago [38], wherein a molecular material absorbs a visible-light photon generating a singlet exciton S which subsequently undergoes a spin-allowed transformation into two triplet excitons TT [39–44]. Nearly a decade ago, it was shown that dynamics of excitons can be altered drastically by embedding them in an optical cavity [26]. The idea of utilizing cavities to enhance SF was later proposed, drawing inspiration from the collective enhancement of SF efficiency observed in acene aggregates [45]. Then the pivotal role of the

*Electronic address: YZhao@ntu.edu.sg

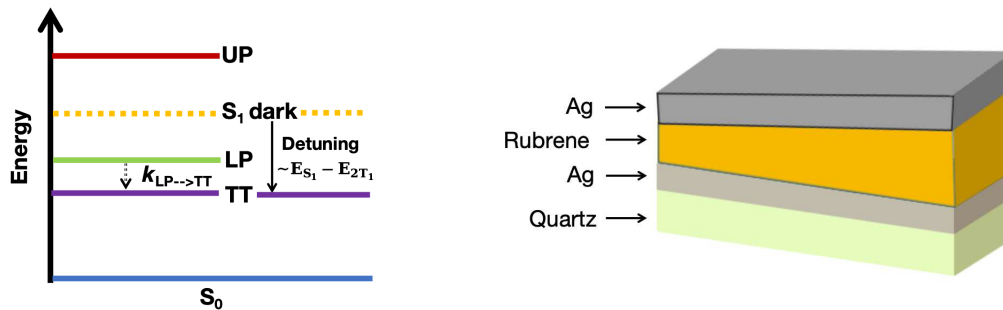


Figure 1: PPP-mediated SF. A collective bright singlet state coupled to the cavity mode forms the LP and UP states, while the collective singlet dark states are decoupled from the cavity mode. (a) Energy diagram illustrating the initial step of the SF process in the presence of collective strong coupling. The LP efficiently channels population towards the TT state. (b) A schematic illustration of the slanted rubrene microcavity [47].

Table I: Summary of bare SF material parameters and their optimal gain rates of TT yield $\tilde{\epsilon}_{\text{TT}}/\epsilon_{\text{TT}}$ in the cavity. where ΔG is given by $\Delta G = \omega_{\text{TT}} - \omega_{\text{S}_1}$, and ϵ_{TT} ($\tilde{\epsilon}_{\text{TT}}$) represents bared (polariton-assisted) TT yield, respectively.

Molecule	$\Delta G(\text{meV})$	$\epsilon_{\text{TT}}(\%)$	$\tilde{\epsilon}_{\text{TT}}/\epsilon_{\text{TT}}$	Ref.
Tetracene	150	0.01	~ 16	[45]
Pentacene	-110	100	~ 1.4	[45]
Hexacene	-630	48	~ 3.3	[45]
Rubrene	50	17, 40, > 99.9	~ 1.3	[47–49]

formally dark states for the amplification of SF in the strong-coupling regime in organic materials was demonstrated [46].

Figure 1 sketches the essentials of the cavity-enhanced SF, showing the lower polaritonic (LP) state and the upper polaritonic (UP) state producing via the coupling of the SF dimer to the cavity. Considering the large density of states in the manifolds of dark and TT states, it is essential that the TT states have to be energetically lower than the dark states, in order to prevent population leakage and enhance the SF yield (panel a). Hence the LP state acts as a new channel towards the TT state to accelerate SF. Figure 1(b) depicts the optical microcavity, in which the rubrene amorphous film is sandwiched between two silver mirrors for producing polaritonic states [47]. By constructing the slanted rubrene microcavity, Takahashi *et al.* experimentally demonstrated the polaron decoupling effect [47] theoretically predicted by Spano [27]. They also found three critical parameters governing the cavity-mediated SF, the excitonic fraction in the LP state, the energy alignment between the LP and TT states, and the Frank-Condon factor for the excitation [47].

The parameters characterizing several popular bare and cavity-manipulated SF materials are listed in Table I.

As follows from this Table, incorporation of these materials in microcavities increases SF yield. Hence integration of QED-cavities into the design of photovoltaic devices offers a notable potential to enhance singlet-to-triplet conversion efficiency and circumvent the Shockley-Queisser limit [50, 51]. However, the fulfilment of this program requires understanding of the microscopic mechanisms of the cavity-enhanced SF. In this context, it is essential that the majority of the SF materials (for example, pentacene [52, 53], tetracene [54, 55], and rubrene [56]) exhibit conical-intersection (CI) driven SF.

CIs are points of degeneracy in the potential energy surfaces (PESs) of isolated polyatomic molecules. Manifolds of these points of degeneracy, known as CI seams, undermine the Born-Oppenheimer approximation and open up effective and fast channels for the population and charge transfer [57]. In PPP systems, the situation is complicated by the fact that CIs may be either intrinsic or cavity-induced [58, 59]. In the strong coupling regime, an intrinsic molecular CI splits into a pair of polaritonic CIs [60, 61]. Furthermore, strong coupling to the cavity mode may produce so-called light-induced CIs [62, 63], which occur even in diatomic molecules possessing no intrinsic CIs [64, 65]. These light-induced CIs may be caused by the presence of additional (for example, rotational/orientational) DOFs. Hence the coupling to the cavity creates multidimensional PES landscapes comprising cascades of intrinsic and cavity-induced/modified CIs [60, 61, 66–71]. On the one hand, this enormously complicates the situation and imposes high requirements on the numerical efficiency and accuracy of the theoretical methods used for the simulation of dynamic and spectroscopic responses of these systems. On the other hand, the cavity-induced/modified CIs create additional pathways and shortcuts for the population transfer, which can be used for engineering/optimizing the SF process [61, 67]. Yet, the polaritonic CIs in the strong-coupling regime may act as double-edged sword. For example, Gu *et al.* uncovered that SF can be significantly suppressed, since polaritonic CIs are shifted away

from the Franck-Condon region in pentacene dimers [60]. Hence enhancing the SF process in cavities remains a topic of contention.

In this Perspective, we summarize the status quo of the studies into the CI-driven cavity-mediated SF from the point of view of theoreticians. We begin with the overview of the fundamental processes shaping the SF mechanisms and outline spectroscopic signatures of these mechanisms. Then we put these findings in the general context of theoretical studies of PPP molecular systems and materials, outlining the open questions and computational challenges. For making the present work reader-friendly, we choose to concentrate on a single representative SF system, viz. rubrene dimers (RDs). All simulations of the present work were performed with the multiple Davydov Ansatz (mDA) method [72, 73] which is a well-established many-body wave-function-based variational integrator of quantum dynamics employing Gaussian coherent states (see the last section of this work for the discussion of the suitable numerical tools for the simulation of PPP dynamics and spectroscopy). If the mDA multiplicity is high enough (this is so for all numerical illustrations of the present work), the mDA can be regarded as the numerically accurate method which faithfully reproduces evolutions of quantum systems with many DOFs.

Polaritonic CI landscapes. In rubrene, the energy of the TT state, E_{TT} is slightly higher than the energy of the singlet state, E_{S_1} . Hence SF – without thermal activation [56] or without excitation to higher-lying electronic states E_{S_n} [74] – is rather inefficient. Furthermore, the usual mechanism of polaritonic enhancement of SF through the cavity-finetuned resonance of the LP and TT states, is ineffective in rubrene, too [1, 45, 47]. Hence rubrene is a suitable system for exploring novel cavity-induced mechanisms of the SF enhancement.

Following Ref. [61], we consider a microcavity with one or two RDs placed into it. To focus on the net effect of the cavity-induced control mechanisms, the loss of photons in the cavity is neglected. This is justified, since the ultrahigh-Q PhCnB cavities ($Q \sim 750,000$) have been created by using a five-hole taper design [75] and the timescale of the studied processes (hundreds of femtoseconds) is quite short.

In this section, the j th RD participating in the CI-mediated SF is modeled as a system with three electronic states (the ground state $S_0^{(j)}$, the singlet excited state $S_1^{(j)}$, and the correlated triplet pair state $\text{TT}^{(j)}$) and two vibrational modes (the tuning mode with a frequency $\Omega_t = 0.186$ eV and coordinate $Q_t^{(j)}$, and the coupling mode with a frequency $\Omega_c = 0.0154$ eV and coordinate $Q_c^{(j)}$) [56, 61]. The electronic energies of the singlet and triplet states are fixed at $E_{\text{S}_1}^{(j)} = 2.23$ eV and $E_{\text{TT}_1}^{(j)} = 2.28$ eV. The cavity is modelled via a single photonic mode of a frequency $\omega_c = 2.256$ eV, which is nearly in the electronic resonance with the $S_1^{(j)}$ and

$\text{TT}_1^{(j)}$ states. Ω determines the coupling of the RDs to the cavity mode. If not explicitly stated otherwise, we set $\Omega = 0.2$ eV, which corresponds to the strong cavity-RD coupling regime. To increase space of the adjustable parameters, the rotating-wave approximation (RWA) in the description of the cavity-matter interaction was not applied.

All levels of the combined RD(s) + cavity system can be classified according to the expectation value of the number operator

$$N = \langle \Psi_n(\mathbf{Q}) | \hat{N}_{\text{ex}} | \Psi_n(\mathbf{Q}) \rangle \quad (1)$$

where $|\Psi_n(\mathbf{Q})\rangle$ is the adiabatic eigenfunction of the polaritonic Hamiltonian. N specifies the excitation manifold of the polaritonic PESs. For example, $N = 0$ corresponds to the collective ground state, $N = 1$ yields the singly-excited manifold, etc. To characterize and visualize various states, it is elucidating to introduce several quantifiers. For instance,

$$W_{\text{ph}} = 1 - \sum_{\mathbf{k}} \sum_{n_c \neq 0} |\langle \mathbf{k}, n_c | \Psi_n(\mathbf{Q}) \rangle|^2 \quad (2)$$

gives a fraction of the pure photonic excitation in a certain manifold N . The sum in Eq. (2) runs over the components $k_j = S_1^{(j)}, \text{TT}^{(j)}$ of vector \mathbf{k} . The number of these components matches the number of RDs in the cavity, and n_c is the quantum number specifying the photonic-mode excitation. Similarly, the TT component of the polaritonic state can be defined as

$$W_{\text{TT}} = \sum_{\mathbf{k} \in \text{TT}} \sum_{n_c} |\langle \mathbf{k}, n_c | \Psi_n(\mathbf{Q}) \rangle|^2, \quad (3)$$

where the notation $\mathbf{k} \in \text{TT}$ means that at least one of the components k_j must contain $\text{TT}^{(j)}$.

The fractions of the TT states (W_{TT} of Eq. (3)) and photonic states (W_{ph} of Eq. (2)) give a convenient visualization of the polaritonic PESs, which is implemented through the line color coding in Figure 2. Panels (a, b) represent a single RD in the cavity, and show the cut of the polaritonic PESs along the symmetric tuning mode Q_t at $Q_c = 0$. Panel (a) corresponds to a cavity-free RD. Hence, $S_1^{(1)}$ and $\text{TT}^{(j)}$ are not dressed with the cavity mode, and only the intrinsic RD CI at $Q_t = 0.07, E = 2.256$ eV exists in this case. It follows that this CI located in the Franck-Condon region provides the only SF pathway. In the presence of cavity, the PESs change substantially, and cascades of polaritonic CIs appear in Figure 2(b). As the coupling to the cavity increases, the two polaritonic CIs move away from the Franck-Condon point, the distance between the pair of polaritonic CIs increases with N , and positions of these CIs lie along the V-shaped dash lines in Figure 2(b). It is essential that the fraction of the hybrid matter-photon PESs increases with N near the Franck-Condon point. This facilitates the cavity-assisted SF.

The cuts of PESs for two RDs strongly coupled to the cavity mode are shown in Figures 2(c) (highlighting the

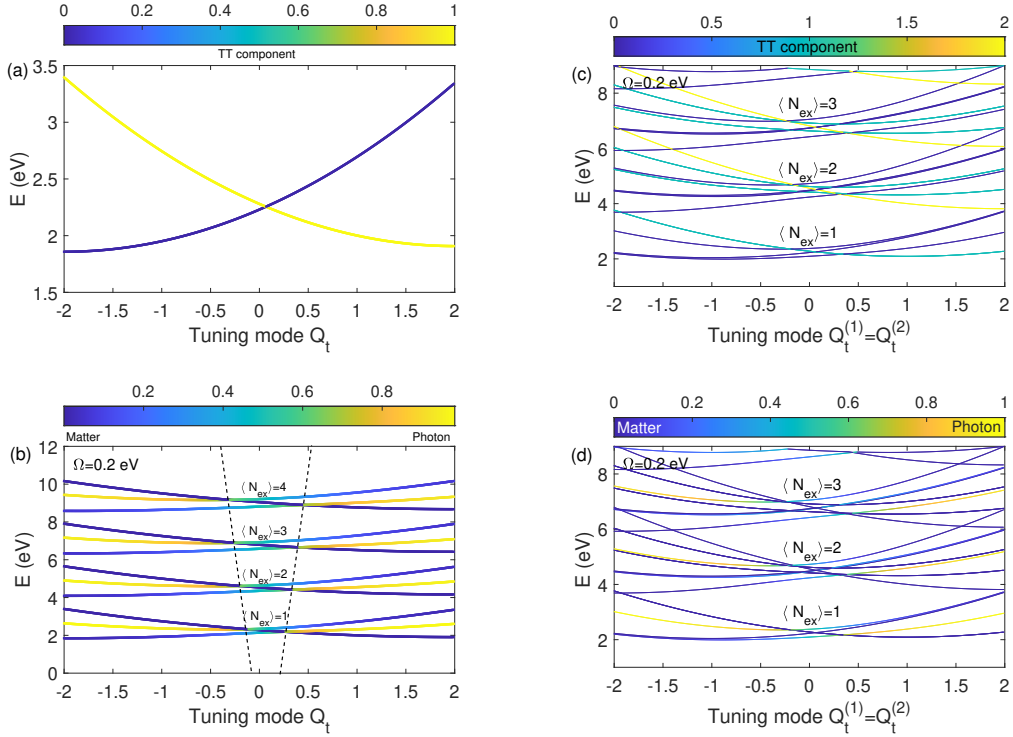


Figure 2: Cuts of the adiabatic PESs along the tuning mode ($Q_c^{(j)} = 0$) for one (left column; panels a, b) and two (right column; panels c, d) RDs in the cavity for the first few polaritonic manifolds N . (a) No coupling to the cavity mode ($\Omega = 0$), the bare CI is located in the Franck-Condon region at $Q_t^{(1)} = 0.07$, $E = 2.256$ eV. (b, c, d) Strong coupling to the cavity mode ($\Omega = 0.2$ eV). The fraction of the TT states (W_{TT} of Eq. (3)) is indicated through the line color coding of PESs (a, c), while fraction of the photonic states (W_{ph} of Eq. (2)), is indicated through the line color coding of the PESs (b, d). The dash lines in panel (b) show positions of the polaritonic CIs.

TT character of the PESs) and (d) (highlighting the photonic character of the PESs). First of all the number of the coupled PESs apparently increases with the number of RDs in the cavity. If for a single RD we have 3 PESs for $N \geq 1$, for two RDs there are 5 PESs for $N = 1$, and 9 PESs for $N \geq 2$. The PES with the CIs at $Q_t^{(1)} = Q_t^{(2)} = 0.07$ eV, which corresponds to both RDs in the triplet state, exists for all N . With the exception of this PES, the cavity-RD coupling repels polaritonic CIs from the central region, but the effect is not so pronounced as in the case of a single RD.

SF Dynamics Mediated by Polaritonic CIs. Let us explore how the polaritonic PESs coupled through cascades of the cavity-induced CIs affect the SF dynamics. For this to achieve, it is worthwhile to study what is the impact of the initial excitation of the photonic mode on the ensuing singlet-to-triplet population transfer. In our simulations, the cavity mode is assumed to be initially, at $t = 0$, in the coherent state

$$|\mu_1(t)\rangle = \exp(-|\mu_1|^2/2) \sum_{n_c=0}^{\infty} \frac{\mu_1^{n_c}}{\sqrt{n_c!}} |n_c\rangle \quad (4)$$

where μ_1 is the displacement parameter. For a specific n_c , the main contribution to the coherent state gives the

term with $\mu_1(0) = \sqrt{n_c}$. Hence we will systematically study how the initial preparation of the RD system in the manifold N , where the population is initially placed in the singlet state and the cavity mode is in the coherent state with $\mu_1(0) = \sqrt{N}$ affects SF in the regime of strong RD-cavity coupling. This is illustrated by Figure 3 for one (a, c) and two (b, d) RDs in the cavity.

Let us begin with the considerations of the upper panels, which show the triplet populations for different N . For a single RD, the triplet population – on the average – increases with N up to $N = 6$. For example, the population of ≈ 0.28 is observed at 300 fs for $N = 6$, which is approximately twice larger than the population obtained in the same model without a cavity. However, the SF efficiency starts to decrease at $N = 7$ and is fully suppressed for $N \geq 8$. This effect can be rationalized from the different points of view. On the one hand, it can be viewed as excitation localization on the singlet state $S_1^{(1)}$ and on the photonic mode, which renders the $\text{TT}^{(1)}$ effectively decoupled and the SF switched off (see Refs. [76, 77] for engineering of long-lived localized states in the cavity-QED systems). A qualitatively similar localization is realized, for example, in the spin-boson model in the regime of the strong coupling of the spin system to the bosonic bath

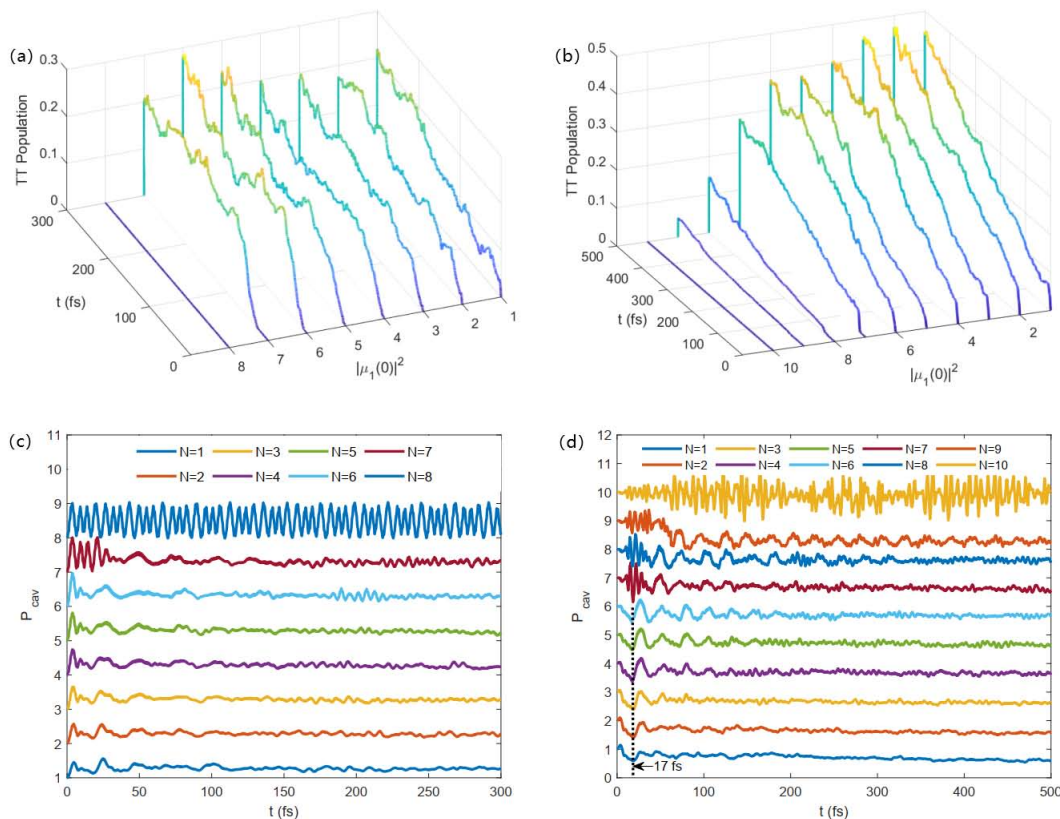


Figure 3: Population dynamics of the triplet state (upper panels) and average photon mode populations $P_{cav}(t)$ (lower panels) for several initial photon-mode pumping numbers $|\mu_1(0)|^2 = N$. Left column (panels a, c): one RD. Right column (panels b, d): two RDs.

[78], even at different system preparations [79]. Alternatively, the effect can be envisaged as an effective annihilation of the nonadiabatic coupling between the singlet and triplet states [80]. It operates through the combined effect of the cavity field (through Rabi cycling) the system itself (through the intrinsic $S_1^{(1)} - TT^{(1)}$ CI), since the photonic mode does not directly couple the singlet and triplet states. Note also that the population evolution of the triplet states starts not from $t = 0$, but from a characteristic time τ_N which increases with N . This indicates that the wavepacket needs $\approx \tau_N$ to reach the polaritonic CIs.

A qualitatively similar situation takes place for 2 RDs in the cavity (Figure 3(b)), with a notable modifications though. For $N = 1$, the total triplet population reaches ≈ 0.45 at $t = 500$ fs, which is ≈ 1.5 higher than for $N = 0$. As demonstrated in the previous section (Figures 2(c, d)) photonic mode helps to generate multiple polaritonic CIs in the Franck-Condon, owing to the elevated number of the coupled cavity-induced CIs and existence of the doubly-excited states in the manifolds N . This cooperativity facilitates the population transfer, inaugurating the onset of the cavity-assisted SF. A comparable relatively high total triplet population is obtained with $N = 2$ (the largest) and with $N = 3$, which is at-

tributed to similar polaritonic PESs for $N = 1, 2, 3$. As shown in Figure 2(c, d), elevated N do not substantially shift positions of the coupled CIs in the Franck-Condon region. Therefore, at variance with the case of a single RD, no SF enhancement with N is essentially observed. On the contrary, as the photon displacement increases, the $TT^{(1)}$ decoupling becomes more pronounced, which results in decreasing triplet populations and, eventually, a full SF switching-off at $N = 10$. This triplet population decrease can be attributed to the influence of the central polaritonic CI (Figure 2(c, d)) which does not exist in the single-RD system (Figure 2(a, b)).

Let us now inspect evolutions $P_{cav}(t)$ of the cavity-mode populations vs. the initial photon pumping numbers N ($P_{cav}(0) = N$) which deliver a complementary information. $P_{cav}(t)$ for a single RD is depicted in Figure 3(c). For N from 1 to 6, the populations exhibit similar behavior: During the first 50 fs, they show several oscillations with a rough period of 22 fs which is related to the tuning mode. Then they reach a quasi-steady-state $\langle P_{cav} \rangle$ value at longer times. It is worth mentioning that $\langle P_{cav} \rangle$ are slightly larger than the initial populations $P_{cav}(0) = N$. It reveals the population redistribution due to the coupling of the cavity mode and the $S_1^{(1)}$ state. $P_{cav}(t)$ for $N = 7$ shows high-amplitude

oscillations during the first ~ 40 fs, which matches the time τ_7 during which the corresponding triplet population in Figure 3(a) is almost zero. For $N = 8$, the high-amplitude oscillations persist over the entire evolution of $P_{cav}(t)$, which is a signature of the localization of the population on the photonic mode and the singlet state, which results in the SF stopping. Interestingly, the period of these fast oscillations reveals the effective Rabi frequency $\Omega_N \approx \Omega\sqrt{N}$ ($2\pi/\Omega_8 \approx 7.3$ fs), which is defined under the assumption that the effective coupling to the cavity scales $\sim \sqrt{N}$.

Figure 3(d) is a counterpart of Figure 3(c), but for two RDs coupled to the cavity. For N from 1 to 6, $P_{cav}(t)$ reach their first local minima at $t \approx 17$ fs (dashed line in panel d), which indicates that a fraction of the photonic-mode population is transferred to the doubly excited electronic states of the RDs. Then, $P_{cav}(t)$ exhibit oscillations with a period of ~ 26 fs, which cannot be directly related to the model parameters. In general, excitation to $1 \leq N \leq 6$ reflects population transfer between photonic mode and excited states of the RDs. For $7 \leq N \leq 9$, $P_{cav}(t)$ shows fast Rabi oscillations at the initial stage, which correlate with the absence of the triplet excitation at the same time interval (cf. Figure 3(b)). For $N = 10$, fast Rabi oscillations spread over the entire $P_{cav}(t)$ evolution, which is the signature of the SF switching-off in Figure 3(b). In the long-time limit, the $P_{cav}(t)$ reach quasi-steady states $\langle P_{cav} \rangle$ the values of which are lower than the initial values $P_{cav}(0)$. This indicates a net population transfer from the photonic mode to the doubly-excited electronic states of RDs.

The above analyses demonstrate that the SF efficiency is primarily determined by two factors. The first factor is the position of the polaritonic CIs (see Figure 2). If the CIs are located in the Franck-Condon region, the subsequent population transfer is facilitated and the higher SF efficiency is achieved. The second factor is the initial wavepacket preparation and the state of the cavity which is controlled by the photonic-mode pumping number $|\mu_1(0)|^2 = N$. This later parameter plays the crucial role, increasing the SF efficiency for small N and fully suppressing SF once N reaches a certain critical value.

Spectroscopic Signatures of Polaritonic CIs. As demonstrated in the previous sections, strong coupling of RDs to the cavity mode drastically alters the SF efficiency owing to the cohesive action of the cavity-induced and intrinsic CIs. This processes are imprinted into non-linear femtosecond spectroscopic responses of these systems. To find spectroscopic signatures of the polaritonic SF occurring in multidimensional PES landscapes, the signals must be accurately simulated and adequately interpreted. For this to achieve, it is essential to realistically model RDs. Indeed, all third-order spectroscopic responses consist of three contributions, the ground-state bleach (GSB), the stimulated emission (SE), and the excited-state absorption (ESA) [81, 82]. The GSB and SE reflect the photoinduced processes in the manifolds with $N = 0$ (the ground state) and $N = 1$ (singly-

excited states), while ESA involves also the doubly-excited states, $N = 2$. Hence modeling individual RDs as systems containing only singly-excited states $S_1^{(j)}$ and $TT^{(j)}$ is insufficient: we have to include higher-excited states $S_n^{(j)}$ and $TT_n^{(j)}$ [71]. Following [56, 71], we set $E_{S_n}^{(j)} = 4.33$ eV and $E_{TT_n}^{(j)} = 4.68$ eV in our simulations. For two RDs in the cavity, we thus obtain a single ground state, 5 singly-excited states and 15 doubly-excited states which are specified in Fig. 4. The states, in turn, can be subdivided into the matter states ($n_c = 0$, left part of Fig. 4) and hybrid states ($n_c > 0$, right part of Fig. 4).

Here we consider electronic two-dimensional (2D) spectra, because electronic 2D spectroscopy (2DES) is one of the most powerful and information-rich third-order spectroscopic techniques (see [83] and references therein). Qualitatively, 2DES spectra $S(\omega_\tau, T_w, \omega_t)$ can be envisaged as a T_w -dependent 2D (ω_τ, ω_t) maps, which reveal correlations between the states of the system excited at a frequency ω_τ at time zero and probed at a frequency ω_t at time T_w . 2DES spectra $S(\omega_\tau, T_w, \omega_t)$ simulated for the two RD system strongly coupled to the cavity mode are presented in Figure 5 for different population times T_w . From top to bottom, shown are the SE (row (a)), GSB (row (b)), and ESA (row (c)) contributions, as well as the total signal (row (d)).

The SE contribution (row (a)) possesses two pronounced diagonal peaks (DPs) and two cross-peaks (CPs) (similar situation takes place in the purely polaritonic dimer system [84]). The DP1 ($\omega_\tau = 2.297$ eV, $\omega_t = 2.297$ eV) and DP2 ($\omega_\tau = 2.429$ eV, $\omega_t = 2.429$ eV) reveal the middle polariton (MP) and the UP bands, respectively. The low-intensity LP band cannot be reliably identified in the SE 2DES spectrum, because 2DES peak intensities are proportional to the product of four relevant transition dipole moments, in contrast with absorption spectra, which are proportional to the product of two transition dipole moments (see the discussion in Ref. [85]). The CP1 ($\omega_\tau = 2.429$ eV, $\omega_t = 2.297$ eV) and CP2 ($\omega_\tau = 2.297$ eV, $\omega_t = 2.429$ eV) quantify the coupling and polaritonic coherence between the states MP and UP. A weak CP ($\omega_\tau = 2.6$ eV, $\omega_t = 2.429$ eV) at $T_w = 16$ fs reveals the phonon sideband. The shape and intensity of the DPs and CPs depend significantly on the waiting time T_w . The DPs at $T_w = 0$ are predominately elongated perpendicular to the main diagonal, but their elongation turns into parallel at longer population times. A certain similarity of the DPs at $T_w = 0$ and 32 fs shows a significant contribution of the polaritonic beating with a period of ~ 32 fs revealing the energy difference of 0.132 eV between the states MP and UP. The two negative CPs are elongated parallel to the main diagonal. Similar to the DPs, the CPs are also significantly modulated by the MP-UP energy-gap beating. The overall decreases of the intensity of the SE contribution with population time mirrors the CI-mediated population transfer from the bright $S_1^{(j)}$ states to the dark $TT_1^{(j)}$ states and reflects thereby the SF dynamics.

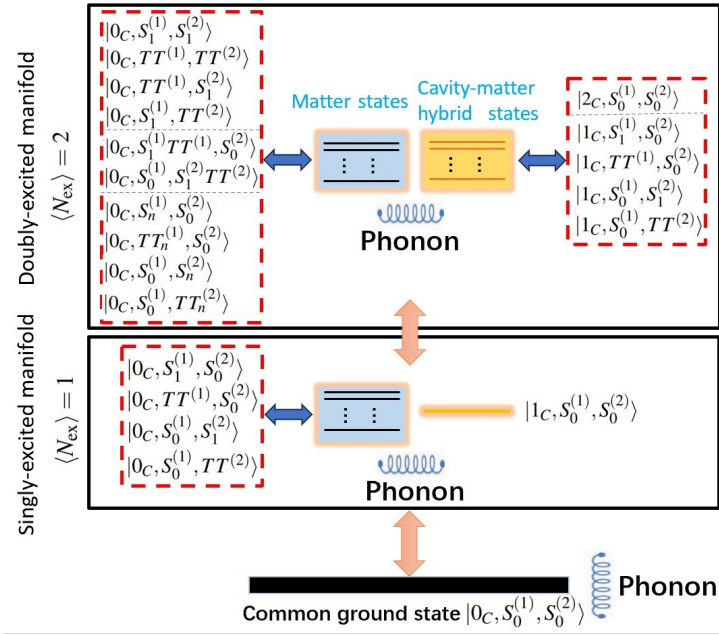


Figure 4: The level structure for two rubrene dimers in the cavity. The superscripts (1) and (2) number the dimers.

The GSB contribution is shown in panels (b) of Figure 5. It reveals the same pairs of the polaritonic DPs and CPs and, additionally, a pair of weaker polariton-phonon CPs, ($\omega_\tau = 2.6$ eV, $\omega_t = 2.429$ eV) and ($\omega_\tau = 2.6$ eV, $\omega_t = 2.297$ eV). In comparison with the SE peaks, their GSB counterparts look rather static. Nevertheless, the GSB contribution reveals the vibrational wave-packet motion in the electronic ground state, which is clearly manifested in the peak evolutions (see Ref. [71]).

The ESA contributions are depicted in panels (c) of Figure 5. The SE and ESA contributions to 2DES spectra reveal photophysical processes in the manifold $N = 1$ [86]. However, the two contributions employ different reporter states for delivering the same information: the SE employs the electronic ground state $N = 0$, while the ESA employs the doubly-excited manifold $N = 2$. Hence shapes and evolutions of predominantly positive SE contributions and predominantly negative ESA contributions are quite similar. Nevertheless, positions of the DPs and CPs in the SE and ESA spectra are slightly shifted with respect to each other. At $T_w = 0$ fs, for example, the (nearly) diagonal ESA peaks are located at ($\omega_\tau \approx 2.297$ eV, $\omega_t \approx 2.317$ eV) and ($\omega_\tau \approx 2.429$ eV, $\omega_t \approx 2.416$ eV). All ESA peaks are elongated parallel to the ω_t axis, due to a high density of states in the manifold $N = 2$. The peak ($\omega_\tau \approx 2.297$ eV, $\omega_t \approx 2.317$ eV), which reveals transitions from the MP state to the states of the doubly-excited manifold, has the highest intensity. Note also that the relative separation between the DPs and CPs along the ω_t axis changes with T_w : cf. the spectra at 0 fs with those at 16 fs. This modulation is caused by the superposition of polaritonic and purely vibrational tuning-mode oscillations. This reflects a higher complex-

ity of the ESA contribution, which involves polaritonic states with $N = 1$ and 2.

Finally, the total 2DES signal $S(\omega_\tau, T_w, \omega_t)$ is shown in Figure 5(d). Since positions of the DPs and CPs in the SE, GSB and ESA contributions nearly coincide, the total 2DES spectrum exhibits positive, negative and dispersed peak shapes, the amplitudes of which are determined by subtle cancellation effects in the superposition of positive SE and GSB contributions and negative ESA contribution. The overall structure of the total 2DES spectra is dominated by the quartet of polaritonic DPs and CPs. In addition, a number of polariton-vibrational peaks around ω_τ or $\omega_t = 2.6$ eV is seen at different T_w . It is remarkable that these hybrid polariton-vibrational peaks are more pronounced in the total signal than in the SE, GSB, and ESA contributions – owing to the aforementioned cancellation effects. The DPs are positive while the CPs exhibit unusual asymmetry: the upper CP is always positive, but the spectral structures around the lower CP can be negative (see the signals for $T_w = 0$ and 16 fs).

Brief summary. We have applied a numerically accurate mDA methodology to explore dynamic and spectroscopic responses of the CI-driven SF RD system strongly coupled to the cavity mode. Several microscopic SF mechanisms have been uncovered, viz. proximity of the CI-driven polaritonic wave packet to the Franck-Condon region, cavity-induced enhancement/weakening/suppression of SF, polaron/polariton decoupling, localization of the singlet-state population via engineering of the cavity-mode excitation, collective enhancement of SF.

Simulation and inspection of nonlinear femtosecond

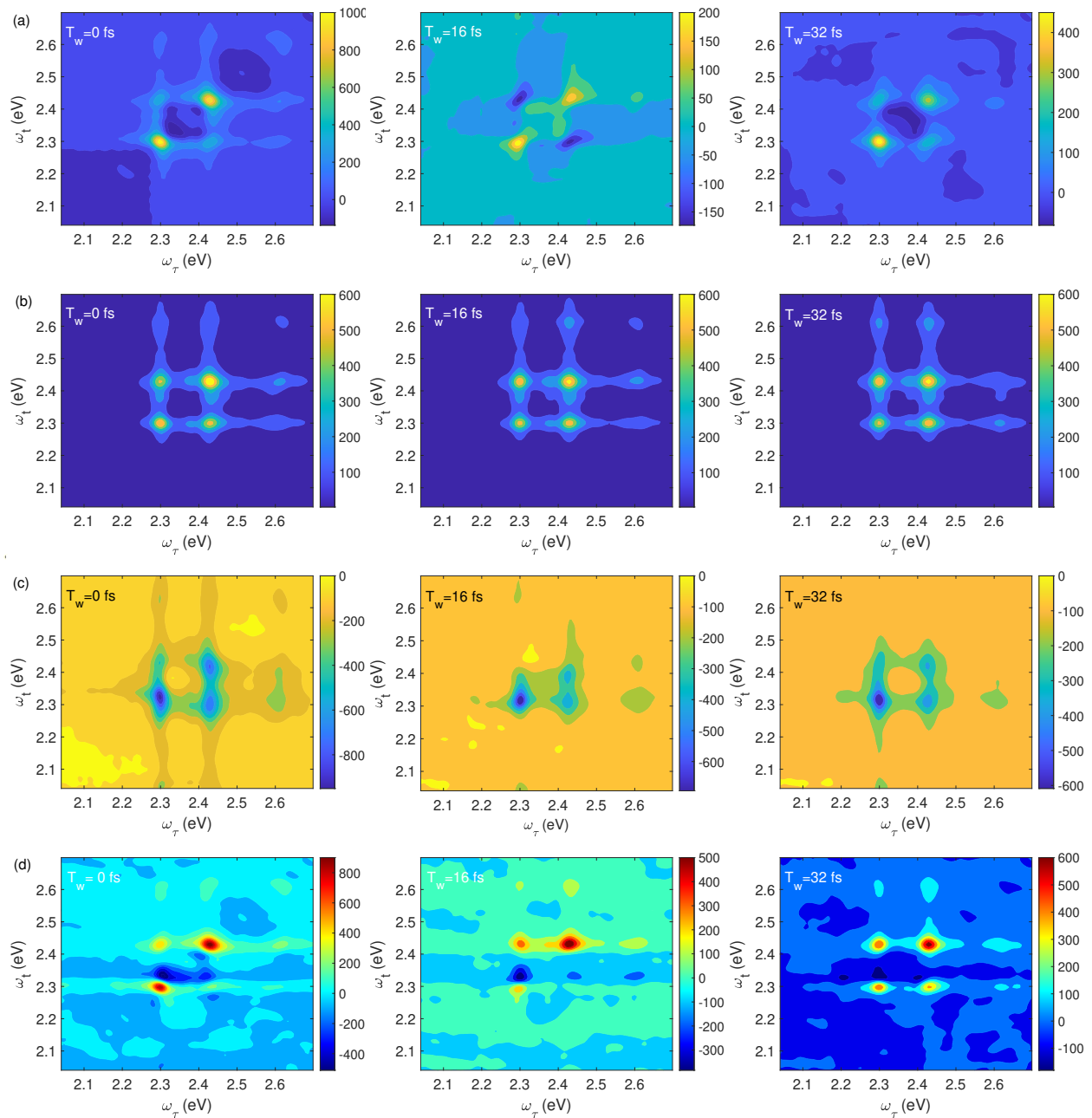


Figure 5: Real part of the SE (row (a)), GSB (row (b)), ESA (row (c)) contributions and the total 2DES spectrum (row (d)) of the two RD system for several population times T_w indicated in the panels. The spectra are computed in the impulsive limit.

spectroscopic signals of the polaritonic CI-SF systems provides accurate information on the singlet-to-triplet transfer in real time. In particular, 2DES spectra of the RD system are dominated by the quartet of DPs and CPs that reveal the MP and UP bands, while the hybrid polariton-vibrational CPs contain information on the UP sideband. This clear separation of the polaritonic and vibrational peaks is a noticeable feature of the obtained spectra. In addition the simulated 2DES spectra exhibit multiple peak-cancellation effects, and their population-time evolution is accompanied by polariton-vibrational

beatings.

We conclude that microcavities can open up new avenues for improving efficiency and stability of the CI-mediated SF, and ultrafast nonlinear spectroscopic signals – if interpreted with adequate theoretical support – can provide the real-time guidance on the SF reaction pathways. Yet, the polaritonic SF studies have not reached its maturity, and a lot of problems await efficient and practical solutions. The specifics are detailed below.

Open questions, challenges, and perspectives.

System Hamiltonian. In excitonic systems, doubly-

excited states are usually understood as the states in which two chromophores are simultaneously excited. This interpretation, however, is not always sufficient for SF aggregates, because polyatomic molecules comprising these aggregates possess dense manifolds of higher-lying excited electronic states and the minimal system supporting the SF reaction is not a single chromophore, but a dimer. Usually, higher-lying electronic states do not contribute to the SF per se (see the discussion below though). Yet, optical transitions between the lower-lying and higher-lying states affect dramatically ESA contributions to spectroscopic signals. Hence higher-lying states of individual molecules comprising SF dimers, aggregates, and materials have to be taken into account in realistic simulations of spectroscopic responses.

It is useful to characterize all relevant electronic states and parameterize the SF Hamiltonians by using ab initio methods of quantum chemistry [87–91]. In addition, ab initio methods can be applied to the entire system of molecules/aggregate+cavity. For example, quantum mechanics/molecular mechanics (QM/MM) simulations of Refs. [92, 93] treat up to 512 polyatomic chromophores in the cavity. Simulations based on the ab initio QED [7, 94], multiple spawning [95], and cavity Born-Oppenheimer Hartree-Fock Ansatz [96] can also provide valuable insight into SF reactions in specific systems.

Quantum dynamic and spectroscopy. Up to now, accurate quantum simulations of up to two CI-carrying molecules/dimers in the cavity have been performed [61, 70, 71]. It is of great interest to push the simulations towards higher number of molecules/dimers N_M and explore how CIs affect cooperativity, e.g., to check the conventional $\sim \sqrt{N_M}$ scaling of the effective system-cavity coupling [97]. For this to achieve, few-molecule models with symmetry-optimized Hamiltonians [98] as well as multi-configuration time-dependent Hartree (MCTDH) [87, 88, 99, 100], tensor-network [101, 102], and mDA methods look promising. Recently emerging emulations of CIs on quantum simulators [103–105] may also be extended in the future to cavity-CI systems.

Disorder is of paramount importance for realistic modeling of CI-driven cavity-mediated SF systems, taking into account that defects/disorder can induce CIs in semiconducting molecular materials [106] and affect significantly polaritonic transport [107, 108]. Temperature is essential, e.g., for activating CI-mediated SI in rubrene [56] and for catalysing reactions in polaritonic systems [25]. The mDA protocol based on the thermo field dynamics (TFD) [109] was recently applied to explore dynamics of the pristine RD [110, 111] and the Holstein-Tavis-Cummings model [112] at finite temperature.

Apart from mDA, MCTDH and variants of tensor-network methods are especially favorable for performing fully-quantum simulations of realistic polaritonic CI-driven SF systems, because they permit the efficient evaluation of nonlinear spectroscopic signals [113, 114] and – by using the TFD methodology [109] and the recipe of Ref. [115] – finite temperature and static disorder can

also be taken care of in the (relatively) computationally inexpensive manner.

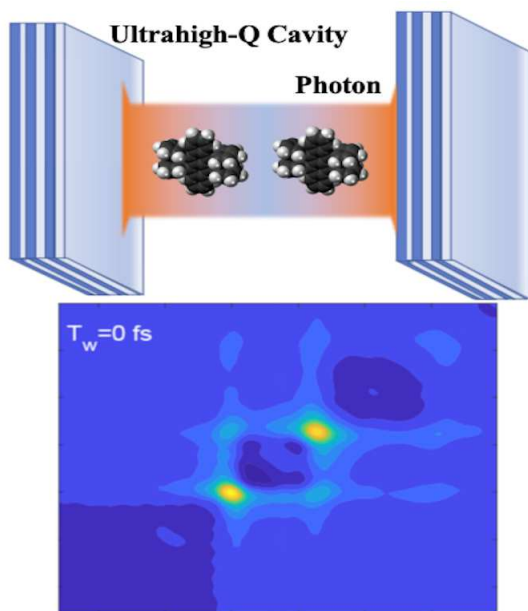
An extra challenge is to identify spectroscopic signatures of polaritonic effects in nonlinear spectroscopic signals of polaritonic CI-driven SF systems. Hence accurate theoretical simulations and interpretations of the existing [47, 116, 117] and forthcoming experiments are demanding but rewarding.

Microscopic mechanisms behind polaritonic CI-driven SF. There exist several methods that can potentially enhance the SF yield. The conventional practices are based on the adjustment of the cavity mode for achieving resonance and strong coupling of the LP or UP states with the triplet state or on the construction of the cavity-assisted SF pathways. On the other hand, the geometric-phase effects may also be harnessed for engineering SF in CI-driven polaritonic systems. The controlling mechanisms may be implemented through collective topological polaritonic phases [118] that are akin to those in topological metamaterials [119]. It is also worthwhile to explore interfacing of light-induced CIs in cavities [120–122] with intrinsic CI systems, as their combination may facilitate fine-tuning of the multiple CI landscapes [123].

Apart from the aforementioned cavity-related mechanisms, there exist other handles for tweaking SF, that are based on the optimization of the bias voltage [124], temperature [56, 125, 126], carrier frequency [127] and intensity [128, 129] of the excitation pulse, or even static disorder [130, 131].

Yet, it is now always clear whether the coupling to the cavity (perhaps in combination with other methods mentioned above) enhances or suppresses the SF yield. It is promising, therefore, to interface the existing protocols for the dynamic simulations of polaritonic CI-driven SF systems with quantum control routines [132, 133], in order to find a robust way to comprehensive optimization of SF in cavities.

I. TOC GRAPHIC



Acknowledgments

The authors gratefully acknowledge the support of the Singapore Ministry of Education Academic Research Fund (Grant No. RG87/20). K. Sun would also like to thank the Natural Science Foundation of Zhejiang Province (Grant No LY18A040005) for partial support. M. F. G. acknowledges support from the National Natural Science Foundation of China (Grant No. 22373028).

-
- [1] Ribeiro, R.F.; Martínez-Martínez, L.A.; Du, M.; CamposGonzalez-Angulo, J.; Yuen-Zhou J. Polariton Chemistry: controlling molecular dynamics with optical cavities. *Chem. Sci.* **2018**, *9*, 6325-6339.
- [2] Climent, C.; Garcia-Vidal, F. J.; Feist, J. Cavity-modified chemistry: towards vacuum-field catalysis. In *Effects of electric fields on structure and reactivity: new horizons in chemistry*. Ed. Shaik, S. and Stuyver, T. Cambridge: Royal Society of Chemistry, **2021**, 343-393.
- [3] Bhuyan, R.; Mony, J.; Kotov, O.; Castellanos, G.W.; Rivas, J.G.; Shegai, T.O.; Båorjesson, K. The Rise and Current Status of Polaritonic Photochemistry and Photophysics. *Chem. Rev.* **2023**, *123*, 10877-10919.
- [4] Sánchez-Barquilla, M.; Fernández-Domínguez, A. I.; Feist, J.; García-Vidal, F. J. A Theoretical Perspective on Molecular Polaritons. *ACS Photonics* **2022**, *9*, 1830-1841.
- [5] Mandal, A.; Taylor, M. A. D.; Weight, B.M.; Koessler, E.R.; Li, X.; Huo, P. Theoretical Advances in Polariton Chemistry and Molecular Cavity Quantum Electrodynamics. *Chem. Rev.* **2023**, *123*, 9786-9879.
- [6] Hirai, K.; Hutchison, J. A. Uji-i, H. Molecular Chemistry in Cavity Strong Coupling. *Chem. Rev.* **2023**, *123*, 8099-8126.
- [7] Ruggenthaler, M.; Sidler, D.; Rubio, A. Understanding Polaritonic Chemistry from Ab Initio Quantum Electrodynamics. *Chem. Rev.* **2023**, *123*, 11191-11229.
- [8] Fassioli, F.; Park, K.H.; Bard, S.E.; Scholes, G.D. Femtosecond Photophysics of Molecular Polaritons. *J. Phys. Chem. Lett.* **2021**, *12*, 11444-11459.
- [9] Gu, B.; Gu, Y.; Chernyak, V. Y.; Mukamel, S. Cavity Control of Molecular Spectroscopy and Photophysics. *Acc. Chem. Res.* **2023**, *56*, 2753-2762.
- [10] Schwinger, J. On quantum-electrodynamics and the magnetic moment of the electron. *Phys. Rev.* **1948**, *73*, 416.
- [11] Feynman, R. P. Space-time approach to quantum electrodynamics. *Phys. Rev.* **1949**, *76*, 769.
- [12] Tomonaga, S.-I.; Oppenheimer, J. R. On infinite field reactions in quantum field theory. *Phys. Rev.* **1948**, *74*, 224.
- [13] Dyson, F. J. The radiation theories of Tomonaga, Schwinger, and Feynman. *Phys. Rev.* **1949**, *75*, 486.
- [14] Orzel, C. Seventy-five years of quantum electrodynamics. *Nat. Rev. Phys.* **2023**, *5*, 700-701.
- [15] Hopfield, J. J.; Thomas, D. G. Polariton Absorption Lines. *Phys. Rev. Lett.* **1965**, *15*, 22.
- [16] Yakovlev, V. A.; Nazin, V. G.; Zhizhin, G. N. The surface polariton splitting due to thin surface film LO vibrations. *Opt. Comm.* **1975**, *15*, 293-295.
- [17] Meschede, D.; Walther, H.; Müller, G. One-Atom Maser. *Phys. Rev. Lett.* **1985**, *54*, 551.
- [18] Rempe, G.; Walther, H.; Klein, N. Observation of quantum collapse and revival in a one-atom maser. *Phys. Rev. Lett.* **1987**, *58*, 353.
- [19] Weisbuch, C.; Nishioka, M.; Ishikawa, A.; Arakawa, Y. Observation of the coupled exciton-photon mode splitting in a semiconductor quantum microcavity. *Phys. Rev. Lett.* **1992**, *69*, 3314.
- [20] Fregoni, J.; Granucci, G.; Coccia, E.; Persico, M.; Corni, S. Manipulating Azobenzene Photoisomerization through Strong Light-Molecule Coupling. *Nat. Commun.* **2018**, *9*, 4688.
- [21] Fregoni, J.; Granucci, G.; Persico, M.; Corni, S. Strong Coupling with Light Enhances the Photoisomerization Quantum Yield of Azobenzene. *Chem* **2020**, *6*, 250°C265.
- [22] Lather, J.; George, J. Improving enzyme catalytic ef-

- iciency by cooperative vibrational strong coupling of water. *J. Phys. Chem. Lett.* **2021**, *12*, 379-384.
- [23] Yang, P.Y.; Cao, J. Quantum Effects in Chemical Reactions under Polaritonic Vibrational Strong Coupling. *J. Phys. Chem. Lett.* **2021**, *12*, 9531-9538.
- [24] Mandal, A.; Krauss, T.D.; Huo, P. Polariton-Mediated Electron Transfer via Cavity Quantum Electrodynamics. *J. Phys. Chem. B* **2020**, *124*, 6321-C6340.
- [25] Campos-Gonzalez-Angulo, J.A.; Ribeiro, R.F.; Yuen-Zhou, J. Resonant catalysis of thermally activated chemical reactions with vibrational polaritons. *Nat. Commun.* **2019**, *10*, 4685.
- [26] Schachenmayer, J.; Genes, Claudio; Tignone, Edoardo; Pupillo, Guido. Cavity-Enhanced Transport of Excitons. *Phys. Rev. Lett.* **2015**, *114*, 196403.
- [27] Spano, F. C. Optical microcavities enhance the exciton coherence length and eliminate vibronic coupling in J-aggregates. *J. Chem. Phys.* **2015**, *142*, 184707.
- [28] Herrera, F.; Spano, F. C. Cavity-Controlled Chemistry in Molecular Ensembles. *Phys. Rev. Lett.* **2016**, *116*, 238301.
- [29] Orgiu, E.; George, J.; Hutchison, J.A.; Devaux, E.; Dayen, J.F.; Doudin, B.; Stellacci, F.; Genet, C.; Schachenmayer, J.; Genes, C.; Pupillo, G.; Samorì P.; Ebbesen T. W. Conductivity in organic semiconductors hybridized with the vacuum field. *Nature Materials*, **2015**, *14*, 1123-1129.
- [30] Mueller, N.S.; Pfitzner, E.; Okamura, Y.; Gordeev, G.; Kusch, P.; Lange, H.; Heberle, J.; Schulz, F.; Reich, S. Surface-Enhanced Raman Scattering and Surface-Enhanced Infrared Absorption by Plasmon Polaritons in Three-Dimensional Nanoparticle Supercrystals. *ACS Nano* **2021**, *15*, 5523-5533.
- [31] Coles, D.M.; Yang, Y.; Wang, Y.; Grant, R.T.; Taylor, R.A.; Saikin, S.K.; Aspuru-Guzik, A.; Lidzey, D.G.; Tang, J.K.H.; Smith, J.M. Strong coupling between chlorosomes of photosynthetic bacteria and a confined optical cavity mode. *Nature Comm.* **2014**, *5*, 5561.
- [32] Tsargorodska, A.; Cartron, M.L.; Vasilev, C.; Kodali, G.; Mass, O.A.; Baumberg, J.J.; Dutton, P.L.; Hunter, C.N.; Törmä, P.; Leggett, G. J. Strong Coupling of Localized Surface Plasmons to Excitons in Light-Harvesting Complexes. *Nano Lett.* **2016**, *16*, 6850-6856.
- [33] Coles, D.; Flatten, L. C.; Sydney, T.; Hounslow, E.; Saikin, S. K.; Aspuru-Guzik, A.; Vedral, V.; Kuo-Hsiang Tang, J.; Taylor, R. A.; Smith, J. M.; Lidzey, D. G. A Nanophotonic Structure Containing Living Photosynthetic Bacteria. *Small* **2017**, *13*, 1701777.
- [34] Schlawin, F.; Kennes, D. M.; Sentef, M. A. Cavity quantum materials. *Appl. Phys. Rev.* **2022**, *9*, 011312.
- [35] Sanvitto, D.; Kéna-Cohen, S. The road towards polaritonic devices. *Nat. Mat.* **2016**, *15*, 1061-1073.
- [36] Wang, Z.; Hu, Y.; Zhang, S.; Sun, Y. Artificial photosynthesis systems for solar energy conversion and storage: platforms and their realities. *Chem. Soc. Rev.* **2022**, *51*, 6704-6737.
- [37] Puntoriero, F.; La Ganga, G.; Cancelliere, A. M.; Campagna, S. Recent progresses in molecular-based artificial photosynthesis. *Current Opinion in Green and Sustainable Chemistry*, **2022**, *36*, 100636.
- [38] Singh, S.; Jones, W. J.; Siebrand, W.; Stoicheff, B. P.; Schneider, W. G. Laser Generation of Excitons and Fluorescence in Anthracene Crystals. *J. Chem. Phys.* **1965**, *42*, 330.
- [39] Smith, M.B.; Michl, J. Singlet Fission. *Chemical Reviews* **2010**, *110*, 6891-6936.
- [40] Smith, M.B.; Michl, J. Recent Advances in Singlet Fission. *Annual Review of Physical Chemistry* **2013**, *64*, 361-386.
- [41] Japahuge, A.; Zeng, T. Theoretical Studies of Singlet Fission: Searching for Materials and Exploring Mechanisms. *ChemPlusChem* **2018**, *83*, 146-182.
- [42] Miyata, K.; Conrad-Burton, F. S.; Geyer, F. L.; Zhu, X.-Y. Triplet Pair States in Singlet Fission. *Chem. Rev.* **2019**, *119*, 4261-4292.
- [43] Reichman, D. R.; Zhu, X. Singlet Fission. *J. Chem. Phys.* **2020**, *153*, 110401.
- [44] Ullrich, T.; Munz, D.; Guldi, D. M. Unconventional singlet fission materials. *Chem. Soc. Rev.* **2021**, *50*, 3485.
- [45] Martínez-Martínez, L.A.; Du, M.; Ribeiro R.F.; Kéna-Cohen, S.; Yuen-Zhou J. Polariton-assisted singlet fission in acene aggregates. *J. Phys. Chem. Lett.* **2018**, *9*, 1951-1957.
- [46] Polak, D.; Jayaprakash, R.; Lyons, T. P.; Martínez-Martínez, L. A.; Leventis, A.; Fallon, K. J.; Coulthard, H.; Bossanyi, D. G.; Georgiou, K.; Petty, A. J.; Anthony, J.; Bronstein, H.; Yuen-Zhou, J.; Tartakovskii, A. I.; Clark, J.; Musser, A. J. Manipulating molecules with strong coupling: harvesting triplet excitons in organic exciton microcavities. *Chem. Sci.* **2020**, *11*, 343.
- [47] Takahashi, S.; Watanabe, K.; Matsumoto, Y. Singlet fission of amorphous rubrene modulated by polariton formation. *J. Chem. Phys.* **2019**, *151*, 074703.
- [48] Ma, L.; Zhang, K.; Kloc, C.; Sun, H.; Soci, C.; Michel-Beyerle, M. E.; Gurzadyan, G. G. Fluorescence from rubrene single crystals: Interplay of singlet fission and energy trapping. *Phys. Rev. B* **2013**, *87*, 201203(R).
- [49] Maslennikov, D.R.; Maimaris, M.; Ning, H.; Zheng, X.; Mondal, N.; Bruevich, V.V.; Pratik, S.M.; Pratik, A.J.; Pratik, V.; Bredas, J.-L.; Coropceanu, V.; Coropceanu, A.A. Interplay Between Mixed and Pure Exciton States Controls Singlet Fission in Rubrene Single Crystals. *arXiv:2308.10593 [cond-mat.mtrl-sci]* **2023**.
- [50] Shockley, W.; Queisser, H. J. Detailed Balance Limit of Efficiency of p-n Junction Solar Cells. *J. Appl. Phys.* **1961**, *32*, 510.
- [51] Markvart, T. *Shockley: Queisser Detailed Balance Limit After 60 Years*. WIREs Energy Environ. **2022**, e430.
- [52] Musser, A. J.; Liebel, M.; Schnedermann, C.; Wende, T.; Kehoe, T. B.; Rao, A.; Kukura, P. Evidence for Conical Intersection Dynamics Mediating Ultrafast Singlet Exciton Fission. *Nat. Phys.* **2015**, *11*, 352-357.
- [53] Duan, H.-G.; Jha, A.; Li, X.; Tiwari, V.; Ye, H.; Nayak, P. K.; Zhu, X.-L.; Li, Z.; Martínez, T. J.; Thorwart, M.; Miller, R. J. D. Intermolecular vibrations mediate ultrafast singlet fission. *Sci. Adv.* **2020**, *6*, eabb0052.
- [54] Morrison, A. F.; Herbert, J. M. Evidence for Singlet Fission Driven by Vibronic Coherence in Crystalline Tetracene. *J. Phys. Chem. Lett.* **2017**, *8*, 1442-1448.
- [55] Wang, G.; Zhang, C.; Liu, Z.; Wang, R.; Ma, H.; Wang, X.; Xiao, M. Singlet Fission Dynamics in Tetracene Single Crystals Probed by Polarization-Dependent Two-Dimensional Electronic Spectroscopy. *J. Phys. Chem. A* **2020**, *124*, 10447-10456.
- [56] Miyata, K.; Kurashige, Y.; Watanabe, K.; Sugimoto, T.; Takahashi S.; Tanaka S.; Takeya, J.; Yanai, T.; Matsumoto, Y. Coherent singlet fission activated by symmetry breaking. *Nat. Chem.* **2017**, *9*, 983-989.

- [57] Domcke, W.; Yarkony, D.R.; Köppel, H. (Eds.). *Conical Intersections: Theory, Computation and Experiment*; World Scientific, Singapore, 2011.
- [58] Bennett, K.; Kowalewski, M.; Mukamel, S. Novel photochemistry of molecular polaritons in optical cavities. *Faraday Discuss.* **2016**, *194*, 259-282.
- [59] Kowalewski, M.; Fingerhut, B. P.; Dorfman, K. E.; Bennett, K.; Mukamel, S. Simulating Coherent Multidimensional Spectroscopy of Nonadiabatic Molecular Processes: From the Infrared to the X-ray Regime. *Chem. Rev.* **2017**, *117*, 12165-12226.
- [60] Gu, B.; Mukamel, S. Optical-Cavity Manipulation of Conical Intersections and Singlet Fission in Pentacene Dimers. *J. Phys. Chem. Lett.* **2021**, *12*, 2052-2056.
- [61] Sun, K.; Gelin, M.F.; Zhao, Y. Engineering Cavity Singlet Fission in Rubrene. *J. Phys. Chem. Lett.* **2022**, *13*, 4090-4097.
- [62] Halász, G. J.; Šindelka, M.; Moiseyev, N.; Cederbaum, L. S.; Vibók, Á. Light-Induced Conical Intersections: Topological Phase, Wave Packet Dynamics, and Molecular Alignment. *J. Phys. Chem. A* **2012**, *116*, 2636-2643.
- [63] Demekhin, P. V.; Cederbaum, L. S. Light-induced conical intersections in polyatomic molecules: General theory, strategies of exploitation, and application. *J. Chem. Phys.* **2013**, *139*, 154314.
- [64] Moiseyev, N.; Šindelka, M.; Cederbaum, L. S. Laser-induced conical intersections in molecular optical lattices. *J. Phys. B: At. Mol. Opt. Phys.* **2008**, *41*, 221001.
- [65] Cseh, A.; Kowalewski, M.; Halász, G. J.; Vibók, Á. Ultrafast Dynamics in the Vicinity of Quantum Light-Induced Conical Intersections. *New J. Phys.* **2019**, *21*, 093040.
- [66] Sun, K. W.; Huang, Z. K.; Gelin, M. F.; Chen, L. P.; Zhao, Y. Monitoring of singlet fission via two dimensional photon-echo and transient-absorption spectroscopy: Simulations by multiple Davydov trial states. *J. Chem. Phys.* **2019**, *151*, 114102.
- [67] Gu, B.; Mukamel, S. Manipulating nonadiabatic conical intersection dynamics by optical cavities. *Chem. Sci.* **2020**, *11*, 1290-1298.
- [68] Cho, D.; Gu, B.; Mukamel, S. Optical Cavity Manipulation and Nonlinear UV Molecular Spectroscopy of Conical Intersections in Pyrazine. *J. Am. Chem. Soc.* **2022**, *144*, 7758-7767.
- [69] Gu, B.; Mukamel, S. Photon Correlation Signals in Coupled-Cavity Polaritons Created by Entangled Light. *ACS Photonics* **2022**, *9*, 938-943.
- [70] Gu, B.; Mukamel, S. Cooperative Conical Intersection Dynamics of Two Pyrazine Molecules in an Optical Cavity. *J. Phys. Chem. Lett.* **2020**, *11*, 5555-5562.
- [71] Sun, K.; Gelin, M.F.; Zhao, Y. Accurate Simulation of Spectroscopic Signatures of Cavity-Assisted, Conical-Intersection-Controlled Singlet Fission Processes. *J. Phys. Chem. Lett.* **2022**, *13*, 4280-4288.
- [72] Zhao, Y.; Sun, K.; Chen, L.P.; Gelin, M.F. The hierarchy of davydov's ansätze and its applications, *WIREs Comp. Mol. Sci.* **2022**, *12*, e1589.
- [73] Zhao, Y. The hierarchy of Davydov's ansätze: From guesswork to numerically "exact" many-body wave functions, *J. Chem. Phys.* **2023**, *158*, 080901.
- [74] Ma, L.; Zhang, K.; Kloc, C.; Sun, H.; Michel-Beyerle, M. E.; Gurzadyan, G. G. Singlet Fission in Rubrene Single Crystal: Direct Observation by Femtosecond Pump-Probe Spectroscopy. *Phys. Chem. Chem. Phys.* **2012**, *14*, 8307-8312.
- [75] Deotare, P. B.; McCutcheon, M. W.; Frank, I. W.; Khan, M.; Loncar, M. High quality factor photonic crystal nanobeam cavities. *Appl. Phys. Lett.* **2009**, *94*, 121106.
- [76] Sierant, P.; Biedroń, K.; Morigi, G.; Zakrzewski, J. Many-Body Localization in Presence of Cavity Mediated Long-Range Interactions. *SciPost Phys.* **2019**, *7*, 008.
- [77] Dey, A.; Kulkarni, M. Engineering Indefinitely Long-Lived Localization in Cavity-QED Arrays. *Phys. Rev. A* **2020**, *101*, 043801.
- [78] Wu, N.; Duan, L.; Li, X.; Zhao, Y. Dynamics of a two-level system under the simultaneous influence of a spin bath and a boson bath. *J. Chem. Phys.* **2013**, *138*, 084111.
- [79] Chen, L.; Yan, Y.; Gelin, M. F.; Lü, Z. Dynamics of the spin-boson model: The effect of bath initial conditions. *J. Chem. Phys.* **2023**, *158*, 104109.
- [80] Gelin, M. F.; Egorova, D.; Domcke, W. Manipulating electronic couplings and nonadiabatic nuclear dynamics with strong laser pulses. *J. Chem. Phys.* **2009**, *131*, 124505.
- [81] Mukamel, S.; Abramavicius, D. Many-Body Approaches for Simulating Coherent Nonlinear Spectroscopies of Electronic and Vibrational Excitons. *Chem. Rev.* **2004**, *104*, 2073-2098.
- [82] Valkunas, L.; Abramavicius, D.; Mancal, T. *Molecular excitation dynamics and relaxation: quantum theory and spectroscopy*. John Wiley & Sons, **2013**.
- [83] Biswas, S.; Kim, J. W.; Zhang, X.; Scholes, G. D. Coherent Two-Dimensional and Broadband Electronic Spectroscopies. *Chem. Rev.* **2022**, *122*, 4257-4321.
- [84] Gelin, M. F.; Bondarev, I. V.; Meliksetyan, A. V. Monitoring Bipartite Entanglement in Hybrid Carbon Nanotube Systems via Optical 2D Photon-Echo Spectroscopy. *Chemical Physics* **2013**, *413*, 123-131.
- [85] Krčmar, J.; Gelin, M. F.; Domcke, W. Simulation of Femtosecond Two-Dimensional Electronic Spectra of Conical Intersections. *J. Chem. Phys.* **2015**, *143*, 074308.
- [86] Sun, K.; Xie, W.; Chen, L.; Domcke, W.; Gelin, M. F. Multi-Faceted Spectroscopic Mapping of Ultrafast Nonadiabatic Dynamics Near Conical Intersections: A Computational Study. *J. Chem. Phys.* **2020**, *153*, 174111.
- [87] Reddy, S. R.; Coto, P. B.; Thoss, M. Intramolecular Singlet Fission: Insights from Quantum Dynamical Simulations. *J. Phys. Chem. Lett.* **2018**, *9*, 5979-5986.
- [88] Reddy, S. R.; Coto, P. B.; Thoss, M. Quantum Dynamical Simulation of Intramolecular Singlet Fission in Covalently Coupled Pentacene Dimers. *J. Chem. Phys.* **2019**, *151*, 044307.
- [89] Zhang, B.; Zhao, Y.; Liang, W. Z. Joint Effects of Exciton-Exciton and Exciton-Photon Couplings on the Singlet Fission Dynamics in Organic Aggregates. *J. Phys. Chem. C* **2021**, *125*, 1654-1664.
- [90] Mardazad, S.; Xu, Y.; Yang, X.; Grundner, M.; Schollwöck, U.; Ma, H.; Paecel, S. Quantum Dynamics Simulation of Intramolecular Singlet Fission in Covalently Linked Tetracene Dimer. *J. Chem. Phys.* **2021**, *155*, 194101.

- [91] Jamshidi, Z.; Kargar, K.; Mendive-Tapia, D.; Vendrell, O. Coupling Molecular Systems with Plasmonic Nanocavities: A Quantum Dynamics Approach. *J. Phys. Chem. Lett.* **2023**, *14*, 11367-11375.
- [92] Tichauer, R. H.; Morozov, D.; Sokolovskii, I.; Toppari, J. J.; Groenhof, G. Identifying Vibrations that Control Non-adiabatic Relaxation of Polaritons in Strongly Coupled Molecule-Cavity Systems. *J. Phys. Chem. Lett.* **2022**, *13*, 6259-6267.
- [93] Tichauer, R. H.; Feist, J.; Groenhof, G. Multi-Scale Dynamics Simulations of Molecular Polaritons: The Effect of Multiple Cavity Modes on Polariton Relaxation. *J. Chem. Phys.* **2021**, *154*, 104112.
- [94] Haugland, T. S.; Schäfer, C.; Ronca, E.; Rubio, A.; Koch, H. Intermolecular Interactions in Optical Cavities: An Ab Initio QED Study. *J. Chem. Phys.* **2021**, *154*, 094113.
- [95] Rana, B.; Hohenstein, E. G.; Martínez, T. J. Simulating the Excited-State Dynamics of Polaritons with Ab Initio Multiple Spawning. *J. Phys. Chem. A* **2024**, *128*, 139-151.
- [96] Schnappinger, T.; Kowalewski, M. Ab Initio Vibropolaritonic Spectra in Strongly Coupled Cavity-Molecule Systems. *J. Chem. Theory Comput.* **2023**, *19*, 9278-9289.
- [97] Mandal, A.; Li, X.; Huo, P. Theory of Vibrational Polariton Chemistry in the Collective Coupling Regime. *J. Chem. Phys.* **2022**, *156*, 014101.
- [98] Pérez-Sánchez, J. B.; Koner, A.; Stern, N. P.; Yuen-Zhou, J. Simulating Molecular Polaritons in the Collective Regime Using Few-Molecule Models. *PNAS* **2023**, *120*, No. 15, e2219223120.
- [99] Ulusoy, I. S.; Gomez, J. A.; Vendrell, O. Modifying the Nonradiative Decay Dynamics through Conical Intersections via Collective Coupling to a Cavity Mode. *J. Phys. Chem. A* **2019**, *123*, 8832-8844.
- [100] Ulusoy, I. S.; Vendrell, O. Dynamics and spectroscopy of molecular ensembles in a lossy microcavity. *J. Chem. Phys.* **2020**, *153*, 044108.
- [101] del Pino, J.; Schröder, F. A. Y. N.; Chin, A. W.; Feist, J.; Garcia-Vidal, F. J. Tensor Network Simulation of Non-Markovian Dynamics in Organic Polaritons. *Phys. Rev. Lett.* **2018**, *121*, 227401.
- [102] Fowler-Wright, P.; Lovett, B. W.; Keeling, J. Efficient Many-Body Non-Markovian Dynamics of Organic Polaritons. *Phys. Rev. Lett.* **2022**, *129*, 173001.
- [103] Whitlow, J.; Jia, Z.; Wang, Y.; Fang, C.; Kim, J.; Brown, K. R. Quantum Simulation of Conical Intersections Using Trapped Ions. *Nat. Chem.* **2023**, *15*, 1509-1514.
- [104] Valahu, C. H.; Olaya-Agudelo, V. C.; MacDonell, R. J.; Navickas, T.; Rao, A. D.; Millican, M. J.; Pérez-Sánchez, J. B.; Yuen-Zhou, J.; Biercuk, M. J.; Hempel, C.; Tan, T. R.; Kassal, I. Direct Observation of Geometric-Phase Interference in Dynamics Around a Conical Intersection. *Nat. Chem.* **2023**, *15*, 1503-1508.
- [105] Wang, C. S.; Frattini, N. E.; Chapman, B. J.; Puri, S.; Girvin, S. M.; Devoret, M. H.; Schoelkopf, R. J. Observation of Wave-Packet Branching Through an Engineered Conical Intersection. *Phys. Rev. X* **2023**, *13*, 011008.
- [106] Cohn, B.; Sufrin, S.; Basu, A.; Chuntunov, L. Vibrational Polaritons in Disordered Molecular Ensembles. *J. Phys. Chem. Lett.* **2022**, *13*, 8369-8375.
- [107] Wellnitz, D.; Pupillo, G.; Schachenmayer, J. Disorder Enhanced Vibrational Entanglement and Dynamics in Polaritonic Chemistry. *Commun. Phys.* **2022**, *5*, 120.
- [108] Sun, K.; Dou, C.; Gelin, M. F.; Zhao, Y. Dynamics of Disordered Tavis-Cummings and Holstein-Tavis-Cummings Models. *J. Chem. Phys.* **2022**, *156*, 024102.
- [109] Borrelli, R.; Gelin, M. F. Finite Temperature Quantum Dynamics of Complex Systems: Integrating Thermo-Field Theories and Tensor-Train Methods. *WIREs Comput. Mol. Sci.* **2021**, e1539.
- [110] Sun, K. W.; Xu, Q.; Chen, L. P.; Gelin, M.; Zhao, Y. Temperature Effects on Singlet Fission Dynamics Mediated by a Conical Intersection. *J. Chem. Phys.* **2020**, *153*, 194106.
- [111] Hu, W. J.; Sun, K. W.; Xu, Q.; Chen, L. P.; Zhao, Y. Ultrafast Dynamics in Rubrene and Its Spectroscopic Manifestation. *J. Chem. Phys.* **2020**, *153*, 174105.
- [112] Hou, E.; Sun, K.; Gelin, M. F.; Zhao, Y. Finite Temperature Dynamics of the Holstein-Tavis-Cummings Model. *J. Chem. Phys.* **2024**, in print.
- [113] Gelin, M. F.; Borrelli, R. Simulation of Nonlinear Femtosecond Signals at Finite Temperature via Thermo-Field Dynamics - Tensor Train Method: General Theory and Application to Time- and Frequency-Resolved Fluorescence of the Fenna-Matthews-Olson Complex. *J. Chem. Theory Comput.* **2021**, *17*, 4316-4331.
- [114] Segatta, F.; Ruiz, D. A.; Aleotti, F.; Yaghoubi, M.; Mukamel, S.; Garavelli, M.; Santoro, F.; Nenov, A. Nonlinear Molecular Electronic Spectroscopy via MCTDH Quantum Dynamics: From Exact to Approximate Expressions. *J. Chem. Theory Comput.* **2023**, *19*, 2075-2091.
- [115] Gelin, M. F.; Velardo, A.; Borrelli, R. Efficient Quantum Dynamics Simulations of Complex Molecular Systems: A Unified Treatment of Dynamic and Static Disorder. *J. Chem. Phys.* **2021**, *155*, 134102.
- [116] Mewes, L.; Wang, M.; Ingle, R. A.; Börjesson, K.; Chergui, M. Energy Relaxation Pathways Between Light-Matter States Revealed by Coherent Two-Dimensional Spectroscopy. *Commun. Phys.* **2020**, *3*, 157.
- [117] Takahashi, S.; Watanabe, K. Decoupling from a Thermal Bath via Molecular Polariton Formation. *J. Phys. Chem. Lett.* **2020**, *11*, 1349-1356.
- [118] Pannir-Sivajothi, S.; Stern, N. P.; Yuen-Zhou, J. Molecular and Solid-State Topological Polaritons Induced by Population Imbalance. *Nanophotonics* **2023**, *12*, 3109-3119.
- [119] Ni, X.; Yves, S.; Krasnok, A.; Alù, A. Topological Metamaterials. *Chem. Rev.* **2023**, *123*, 7585-7654.
- [120] Fáabri, C.; Halász, G. J.; Vibók, Á. Probing Light-Induced Conical Intersections by Monitoring Multidimensional Polaritonic Surfaces. *J. Phys. Chem. Lett.* **2022**, *13*, 1172-1179.
- [121] Fáabri, C.; Halász, G. J.; Cederbaum, L. S.; Vibók, Á. Radiative Emission of Polaritons Controlled by Light-Induced Geometric Phase. *Chem. Commun.* **2022**, *58*, 12612.
- [122] Farag, M. H.; Mandal, A.; Huo, P. Polariton Induced Conical Intersection and Berry Phase. *Phys. Chem. Chem. Phys.* **2021**, *23*, 16868.
- [123] Csehi, A.; Vendrell, O.; Halász, G. J.; Vibók, Á. Competition Between Collective and Individual Conical Intersection Dynamics in an Optical Cavity. *New J. Phys.* **2022**, *24*, 073022.

- [124] Tang, X.; Hu, Y.; Jia, W.; Pan, R.; Deng, J.; Deng, J.; He, Z.; Xiong, Z. Intersystem Crossing and Triplet Fusion in Singlet-Fission-Dominated Rubrene-Based OLEDs Under High Bias Current. *ACS Appl. Mater. & Interf.* **2018**, *10*, 1948-1956.
- [125] Li, J.; Chen, Z.; Zhang, Q.; Xiong, Z.; Zhang, Y. Temperature-Dependent Singlet Exciton Fission Observed in Amorphous Rubrene Films. *Org. Electr.* **2015**, *26*, 213-217.
- [126] Zhao, D. X.; O'Connor, J. P.; Schultz, J. D.; Bae, Y. J.; Lin, C.; Young, R. M.; Wasielewski, M. R. Temperature Tuning of Coherent Mixing Between States Driving Singlet Fission in a Spiro-Fused Terrylenediimide. *J. Phys. Chem. B* **2021**, *125*, 6945-6954.
- [127] Bai, Y.; Ni, W.; Sun, K.; Chen, L.; Ma, L.; Zhao, Y.; Gurzadyan, G. G.; Gelin, M. F. Plenty of Room on the Top: Pathways and Spectroscopic Signatures of Singlet Fission from Upper Singlet States. *J. Phys. Chem. Lett.* **2022**, *13*, 11086-11094.
- [128] Ishibashi, Y.; Inoue, Y.; Asahi, T. The Excitation Intensity Dependence of Singlet Fission Dynamics of a Rubrene Microcrystal Studied by Femtosecond Transient Microspectroscopy. *Photochem. Photobiol. Sci.* **2016**, *15*, 1304-1309.
- [129] Cruz, C. D.; Choi, H. H.; Podzorov, V.; Chronister, E. L.; Bardeen, C. J. Photon Upconversion in Crystalline Rubrene: Resonant Enhancement by an Interband State. *J. Phys. Chem. C* **2018**, *122*, 17632-17642.
- [130] Chávez, N. C.; Mattiotti, F.; Méndez-Bermúdez, J. A.; Borgonovi, F.; Celardo, G. L. Disorder-Enhanced and Disorder-Independent Transport with Long-Range Hopping: Application to Molecular Chains in Optical Cavities. *Phys. Rev. Lett.* **2021**, *126*, 153201.
- [131] George, A.; Geraghty, T.; Kelsey, Z.; Mukherjee, S.; Davidova, G.; Kim, W.; Musser, A. J. Controlling the Manifold of Polariton States Through Molecular Disorder. *Adv. Optical Mater.* **2024**, 2302387.
- [132] Shapiro, M.; Brumer, P. *Principles of the Quantum Control of Molecular Processes*. John Wiley & Sons, **2003**.
- [133] Zhang, Y.; Wen, F.; Xiao, M. *Quantum Control of Multi-Wave Mixing*. John Wiley & Sons, **2013**.